Solar Energy Materials & Solar Cells 299 (2026) 114178

Contents lists available at ScienceDirect

Solar Energy Materials and Solar Cells

journal homepage: www.elsevier.com/locate/solmat

Local edge passivation of laser-scribed cells for compensating cut losses

Dheeraj Sah [a,*], Karolis Parfeniukas [b], Roberto Boccardi [c], Narendra Bandaru [a], Agata Lachowicz [d], Bertrand Paviet- Salomon [d], Benjamin Borie [b], Mira Baraket [b], Maksym Plakhotnyuk [b], Gisele A. Dos Reis Benatto [c], Sune Thorsteinsson [c], Peter B. Poulsen [c], Rasmus Schmidt Davidsen [a,**]

[a] Department of Electrical and Computer Engineering (ECE), Aarhus University, Denmark
[b] ATLANT 3D, Mårkærvej 2B, 2630, Taastrup, Denmark
[c] Technical University of Denmark (DTU), Department of Electrical and Photonics Engineering, Frederiksborgvej 399, 4000, Roskilde, Denmark
[d] Swiss Center for Electronics and Microtechnology (CSEM), Rue Jaquet-Droz 1, Neuchâtel, 2000, Switzerland

ARTICLE INFO

Keywords:
Shingle solar cells
Recombination
Edge passivation
Direct atomic layer processing (DALP®)

ABSTRACT

The present work explores the application of Direct Atomic Layer Processing (DALP®) using NANO-FABRICATOR® tool from ATLANT 3D for local edge passivation of laser-scribed cells. Owing to the defects created at the edges by laser scribing, the carrier lifetime decreases significantly in these regions as defects act as recombination centers. To compensate and minimize these losses, a 50 nm blanket layer of TiO_2, using titanium iso-propoxide (TTIP) as precursor and water as co-reactant, was deposited locally using atomic layer deposition (ALD) around the edges, thereby covering the impacted areas. Since the precursor, tunnel oxide passivated contact (TOPCon), solar cells used here were without metallization, the cell parameters like lifetime, lifetime at maximum power point (V_{mpp}), implied open circuit voltage (iV_{oc}) and implied fill factor (iFF) are evaluated in this study. The device is probed using a Sinton WCT120-PL tool and MDP Mapper from Freiberg Instruments for lifetime characterization before and after passivation. Layer deposition followed by annealing lead to a significant improvement of 149 μs in lifetime and a gain of 8.6 mV in implied open circuit voltage (iV_{oc}).

1. Introduction

The deployment of photovoltaic (PV) modules has increased multi-fold recently, especially in the last five years. Global PV installations have now reached 2 tera-watt (TW) out of which 1 TW has been added in the last two years i.e. 2022-2024 [1,2]. Crystalline silicon (c-Si) based solar modules have a market share of >95% in the PV market. This growth is driven by ongoing technological innovations at the cell and module level. At cell level, relatively new solar cell technologies like tunnel oxide passivated contacts (TOPCon), heterojunction thin films (HJT) and interdigitated back contact (IBC) solar cells are marking new heights in power conversion efficiencies. The highest efficiency ever achieved for c-Si based solar cells now stands at 27.8 ± 0.4%, for LONGi's heterojunction thin film back contact (a blend of HJT and IBC designs) cell [3]. However, integration of the cells into modules suffers from optical and electrical losses and gains that change module power as compared to the sum of individual cells [4,5]. These changes are termed the cell-to-module (CTM) ratio. Optical changes originate from reflection of light at different interfaces (glass-encapsulant-cell) and from partial shading from interconnection ribbons and wires. Electrical changes come from the interconnection of the cells. Electrical losses are more significant for larger base wafers (M6 or M10). These wafers generally produce a larger amount of current, which in turn increases resistive losses (proportional to the square of the current) through interconnection. Further, soldering can also cause local heating and pressure causing stress which can eventually lead to micro-cracks [6]. In addition, geometric losses that come from inactive areas between the cells reduce module efficiency. To minimize these CTM resistive losses, PV module technology transitioned from full cell to half-cell [7] and shingle cell technology [8]. Cutting the full cell into half reduces the resistive losses by a factor of four [4], and making shingles i.e. cutting a cell into n small strips in the direction of the current reduces the ohmic losses by $1/n^2$ [9]. Also, shingle module technology offers low ohmic losses, better area utilization (omitting requirement of cell-to-cell gap)

* Corresponding author.
** Corresponding author.
E-mail addresses: dsah@ece.au.dk (D. Sah), rasda@ece.au.dk (R.S. Davidsen).

https://doi.org/10.1016/j.solmat.2026.114178
Received 31 October 2025; Received in revised form 10 January 2026; Accepted 19 January 2026
Available online 23 January 2026

resulting in larger active area within the module which also resulting in better aesthetics [9]. However, to make shingles out of a full cell, cell cutting is required which is usually carried out by laser scribing and mechanical cleaving (LSMC) [10], and in particular thermal laser separation (TLS) [11]. A few studies also employed a 45° rotated wafer [12–14] to obtain smooth surfaces post cutting.

Laser scribing and mechanical cleaving is a two-step process, first a laser is used to scribe grooves on the cell surface and then gentle mechanical force is applied to cleave the cells. Laser scribing ablates the silicon surface leading to melting and re-structuring of silicon along the separation region generating very rough edges [15]. In comparison, TLS results in very smooth edges. TLS utilizes an initial small laser scribe of ~2–3 mm at the edge for crack initiation followed by continuous wave infrared laser (for heating the surface) and a water-air cooling jet generating thermal stress and crack propagation along the guided path [10]. Since TLS leads to cracking the wafer not melting, this method leads to lower crystal defects in the wafer. A laser free alternative to these wafer cutting processes is use of 45° rotated wafers [12–14,16]. In this process, ingots are squared into bricks in a way to align preferred crystallographic planes {110} with cell cutting line. The cutting process is then purely mechanical cleaving and does not require any dedicated laser cutting. Despite the smoothness offered by TLS and 45° rotated wafer methods, all these methods result in degradation of key PV parameters like open-circuit voltage (V_{oc}) and fill factor (FF) owing to increased edge recombination on the raw silicon edges. To minimize these losses, processes such as formation of an emitter window [17] and the edge surface field [18] are performed. Furthermore, different types of atomic layer deposition techniques are utilized to deposit e.g. Al_2O_3 as the edge passivation film, among which notable are thermal atomic layer deposition (T-ALD) [13,19–22], plasma-enhanced ALD (PE-ALD) [22] and spatial ALD [12,23,24]. Other than Al_2O_3, a few studies tested SiN_x:H using plasma enhanced chemical vapor deposition (PE-CVD) [25], H_2 and O_2 plasma using plasma immersion ion implantation (P-III) technique [26] and Nafion using a vacuum spray technique [27,28]. Most of these processes either require special pre-treatment before cutting or coverage of the whole surface including metallic contacts and the active area between grid lines. To avoid this, in this work, we propose local passivation of laser-scribed edges by depositing a passivation layer only around the edge corners and in the edge cross section as shown in Fig. 1. This allows for passivating the damaged surface without altering the properties in the rest of the solar cell surface. Furthermore, annealing of the samples is also carried out to understand the influence of heat treatment on the passivation properties.

2. Experimental

2.1. Laser scribing

We deliberately cut "without metallization" samples into small pieces of varying sizes to understand the impact of laser scribing on the cell pieces. The precursor solar cells used for this work were 135 μm thick, 182 mm × 184 mm size TOPCon solar cells without metallization. These cells were cut into small pieces of size 25 mm × 50 mm using laser scribing and mechanical cleaving. Laser scribing was done from the back side of the solar cell using a nanosecond pulsed fiber laser with a wavelength of 1064 nm and using 56% of the maximum rated power (20 W), with 8–25 laser passes and a scan speed of 215 mm/s. Once scribed, these pieces were separated from the full cells by applying a small pressure, manually, at the edges. The cut pieces were analyzed with a Sinton WCT-120PL tool and microwave detected photoconductivity (MDP) Mapper from Freiberg Instruments to analyze the effect of cutting on minority carrier lifetime. The edges of these pieces were also examined through scanning electron microscope (SEM) to see the morphological changes post laser scribing. After cutting, the exposed edges of these cells were locally passivated from the front side, to treat the junction region. Post passivation, the surface was also examined with energy dispersive spectroscopy (EDS) mapping to confirm the TiO_2 deposition in desired areas. The passivated cells were then re-examined with MDP mapping and Sinton lifetime tester to verify the effectiveness of edge passivation on the lifetime and iV_{oc}, iFF of cells. Passivated samples also underwent annealing at temperatures of 180 °C, 200 °C and 215 °C. Further, five non-passivated samples were also annealed under different temperature conditions to separate out the impact of annealing on bare samples. In addition to these, a sample (Ann_150 °C) underwent the same temperature treatment as the edge-passivated samples did, to trace the temperature impact during deposition on lifetime of a passivated sample.

2.2. Deposition of TiO_2 passivation layer

The local edge passivation was performed using Direct Atomic Layer Processing (DALP®) [29,30] with the NANOFABRICATOR® Lite tool. DALP® represents an atmospheric-pressure, localized analogue of conventional atomic layer deposition (ALD). The spatial separation along with the miniaturized gas nozzle system allows direct patterning of the film through localized delivery of the reactive gases. The spatial separation is achieved by relative motion between the nozzle and the substrate which ultimately defines the deposition pattern on the substrate. Since DALP® works through self-limiting growth mechanism similar to conventional vacuum ALD, it produces films with similar precise control, uniformity and high quality as that of ALD. TiO_2 films with local, well defined rectangular profiles with a surface thickness uniformity variation below 1% are already demonstrated using DALP® [30]. Therefore, the localized nature of DALP® with integrated exceptional film properties of ALD, it is possible to directly deposit a highly conformal passivation layer in the desired areas without altering the surface properties in the non-exposed areas.

Here, titanium dioxide (TiO_2) films were deposited employing titanium isopropoxide (TTIP) as the precursor and water vapor as the co-reactant [31]. The deposition was carried out at a substrate

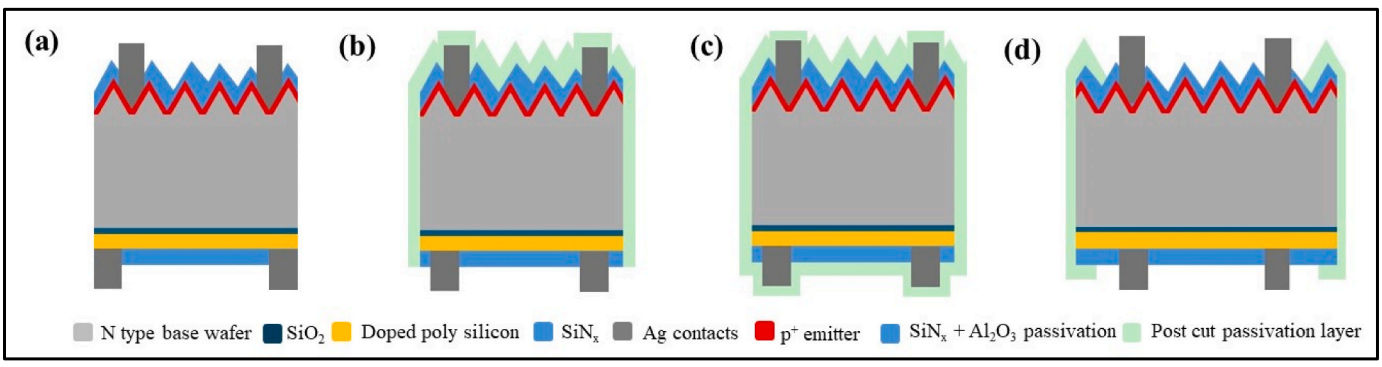

Fig. 1. Sketch of (a) TOPCon solar cell structure, (b) and (c) with usual passivation approaches considered in literature [14,19] and (d) the proposed local edge passivation strategy for this work.

temperature of 150 °C, a regime known to promote amorphous TiO_2 growth [32] with good dielectric quality while preventing crystallization that can degrade passivation performance [33,34]. Deposition was performed selectively along the laser-scribed edges of the TOPCon samples to achieve localized coverage. This approach allowed localized passivation of recombination-active regions without interfering with the bulk surface or front-side optical properties of the device. The targeted thickness of the TiO_2 film was 50 nm. Microscopic inspection confirmed that the deposited layer extended along the edge and partially into the cross-section (~10 μm depth), effectively wrapping the junction region.

Compared with blanket deposition methods [21], DALP® enables precise, conformal growth confined to defect-prone areas. This ensures minimal material usage while preserving the electrical and optical integrity of the non-scribed surfaces. The deposition geometry is illustrated in Fig. 2, where bright regions along the edges correspond to localized TiO_2 growth.

3. Results and analysis

The results are divided into four sections, first a SEM and EDS analysis of the cleaved edges and their elemental composition, then carrier lifetime and iV_{oc} data and the spatial distribution in lifetime maps. Finally, the lifetime results after different annealing temperatures are presented.

3.1. SEM analysis

3.1.1. LSMC surface and its comparison with normal and TLS cut surface

Fig. 3 compares the cross-sectional view of a laser-scribed cleaved edge (Fig. 3(a)) to that of a normal edge (Fig. 3(b)) under SEM. It is seen that under the influence of high laser energy, the silicon surface is damaged, resulting in permanent structural changes at the edges. The impact can be divided into three zones. First, the top part of the rear surface which was under direct impact of the laser beam where the temperature exceeded the melting point of silicon (1414 °C). In this region, the silicon surface is completely melted and solidified with an altered, very rough, microstructure as seen with uneven top back surface in Fig. 3(a). Second, the deep ablation channel observed as V-shaped grooves formed from the direct ablation of silicon and extends all the way out to the front surface of cell. The third zone, re-casted zone visible in the form of spherical granules stuck along the ablated channel walls. The normal edge (Fig. 3(b)), on the other hand, is uniformly smooth and free from structural defects. This contrast clearly indicates the permanent structural changes laser scribing induces onto the silicon surface.

3.1.2. Passivated surface

Fig. 4 displays the SEM image and corresponding EDS mapping of the top surface of a passivated sample post TiO_2 deposition. As can be seen, the deposited TiO_2 layer is distinctly visible on the surface. The TiO_2 layer width was confirmed to be 230–240 μm using ImageJ software. The deposition around the edge was confirmed using EDS mapping. Three different areas viz. the TiO_2 deposited area (top rectangle), non-deposited area (bottom rectangle) and area with both (left rectangle) were considered for the mapping. In the EDS mapping (Fig. 4), Ti and O were observed in the complete top rectangular area, confirming TiO_2 deposition around the edges. In addition, it was observed up to a certain level in the vertical rectangle, effectively highlighting the boundary between deposited and non-deposited areas. Further, no signature of Ti was found on the bottom rectangle, confirming that the TiO_2 deposition was localized in nature i.e. present only along the corner of edges. The surface structure of the TiO_2 exposed area is further shown in Fig. 5.

Fig. 5 shows the magnified secondary electron image with corresponding EDS mapping of the TiO_2 deposited area. The image shows that the random pyramids in this area appear to have a brighter colored coating on top of them, which EDS mapping confirmed to be of TiO_2. In addition to the surface, TiO_2 deposition can be confirmed up to a distance of ~10 μm from the top i.e. the deposited layer effectively covers the top p-n junction as well (Fig. 6).

3.2. Passivation results

Table 1 provides the corresponding values of the observed lifetime for a passivated sample at a carrier injection of 1×10^{15} cm^{-3}, lifetime at V_{mpp}, iV_{oc} and iFF. Before passivation, the device had a lifetime of 724 μs which increased to 823 μs after passivation exhibiting a gain of 99 μs (Fig. 7). Similarly, iV_{oc} and iFF value also increased from 715.0 mV to 717.1 mV and 84.824%–85.120% with corresponding gain of 2.1 mV and 0.296% (absolute), respectively. The sample was then annealed at 180 °C for 10 min and the lifetime values were measured. Right after annealing, the lifetime at 1×10^{15} cm^{-3}, lifetime at V_{mpp} and iV_{oc} values were slightly increased, with corresponding gains of +50 μs, +66 μs and +6.5 mV, respectively. The sample was then annealed at 200 °C, and a decrease in the device parameters was observed. After annealing at 200 °C, the lifetime was decreased by 73 μs at 1×10^{15} cm^{-3}, by 86 μs at V_{mpp}, and iV_{oc} was decreased by 3.5 mV and iFF by 0.025%. These parameters, except iV_{oc}, were further decreased after annealing at 215 °C (Table 1). This observation suggests that the deposition of a 50-nm-thin TiO_2 blanket layer at 150 °C followed by annealing at 180 °C for 10 min resulted in the best device performance. As in this region, gains of 148.36 μs in lifetime, 160.98 μs in lifetime at V_{mpp} and 8.6 mV in iV_{oc} are observed for the device. However, a small decrease of ~0.1% in iFF is observed.

3.3. Lifetime mapping results

The lifetime mapping along with the corresponding histogram highlighting the impact of passivation and annealing on the sample

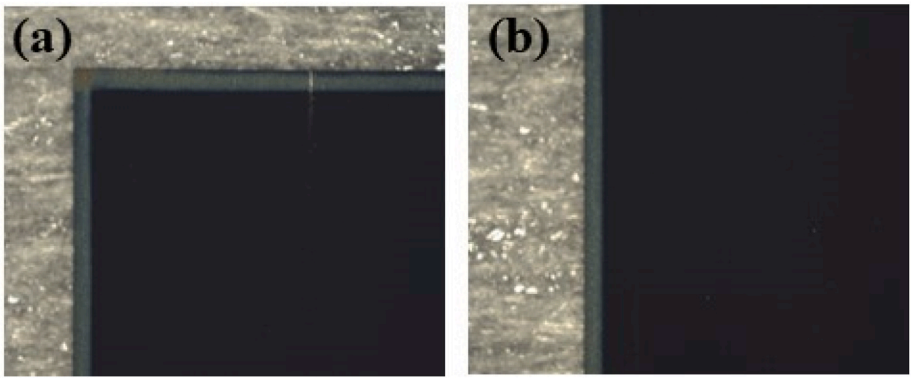

Fig. 2. Optical microscope images (not to scale) of the top surface of passivated cells. The bright line showing the local TiO_2 deposition (a) around the corner (b) along the edge.

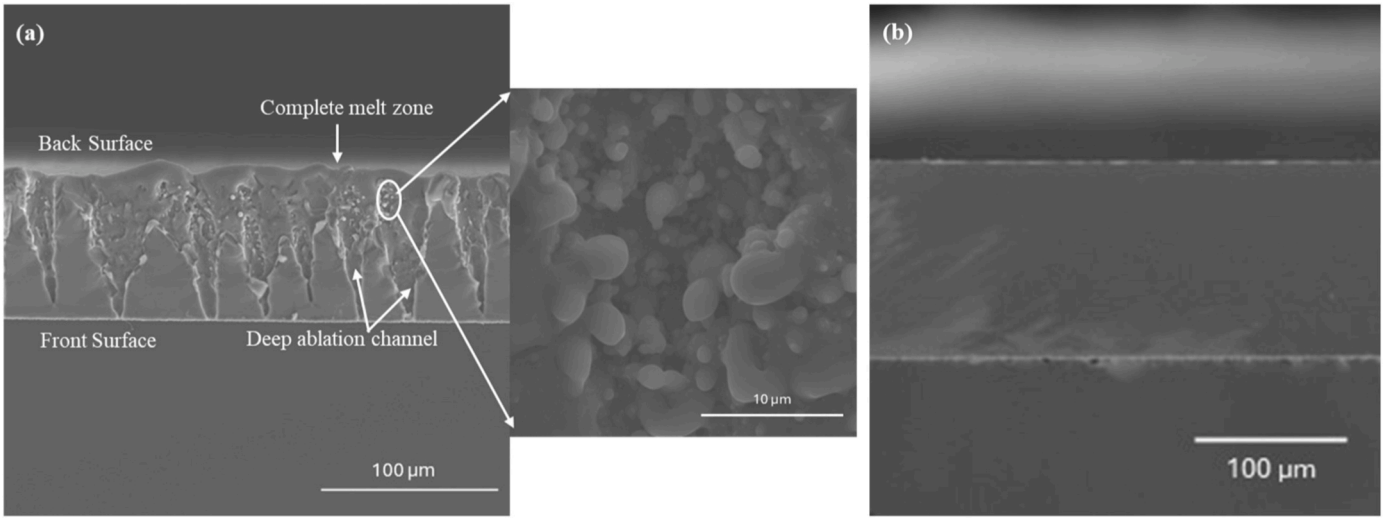

Fig. 3. Cross sectional SEM images: (a) laser-scribed cleaved edge (b) normal edge of silicon solar cell.

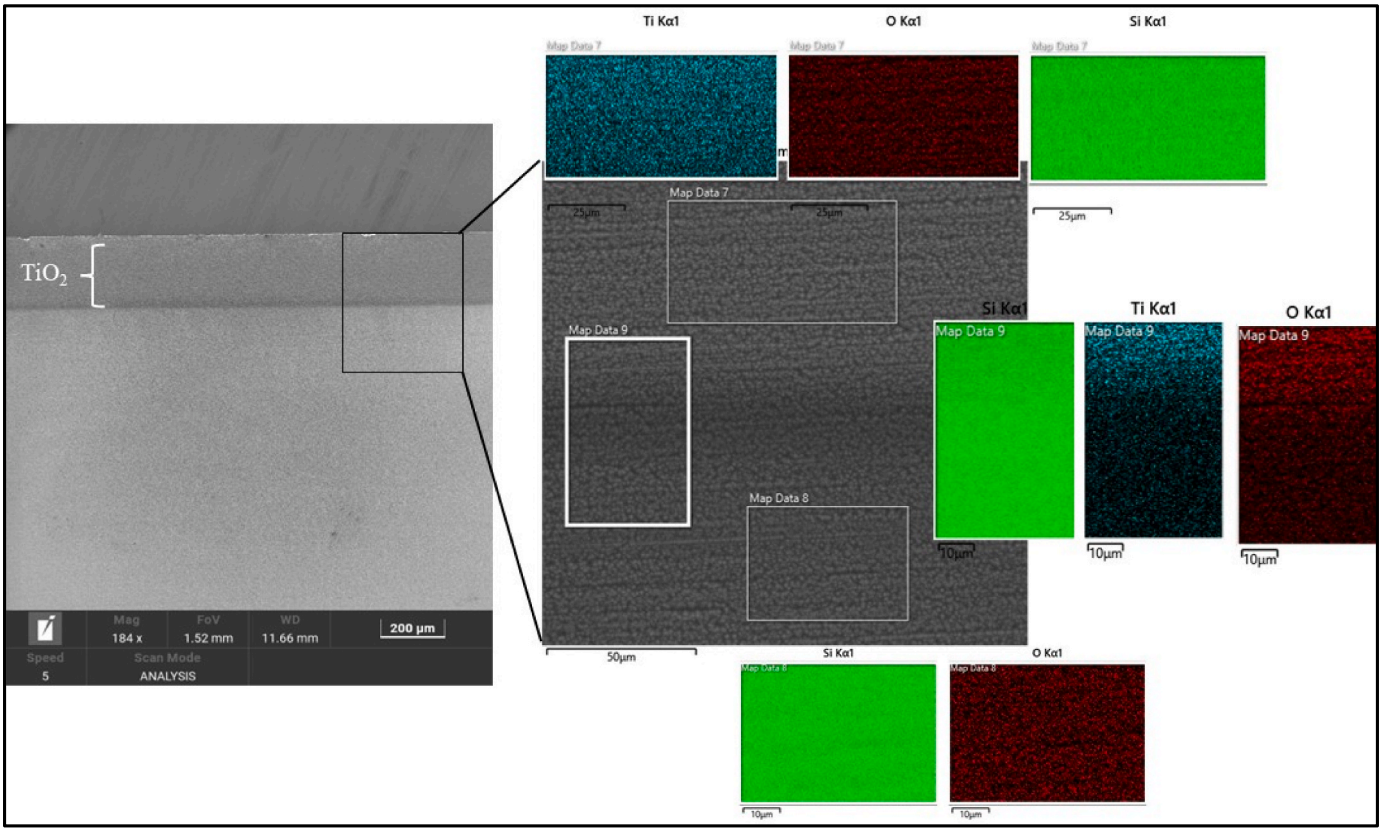

Fig. 4. SEM image (left) top-view of front surface after localized TiO_2 deposition and corresponding EDS elemental mapping (right) of three different regions of a passivated sample. SEM image indicating the clear contrast between TiO_2 deposited area to the rest of the surface and EDS mapping confirming the spatial distribution of TiO_2.

lifetime are shown in Fig. 8. It is observed that the laser scribing (Fig. 8 (a)) leads to severe damage in the cell, as the lifetime decreases to ~50–100 µs at the edges (shown by red color around the edges) and furthermore, lifetime in the rest of the sample is limited to around 300–400 µs (shown by green color). After passivation, two clear changes are observed in the lifetime map. First, the width of red color around the edges is narrowed down to some extent, showing the efficient suppression of recombination centers in these regions. Second, the lifetime at the center region also increased to 550–580 µs, as shown by sky blue-blue region at the center, which clearly suggests that the wrapping around the defected area (edge corners and cross section to some extent) reduces the edge recombination caused by the laser scribing. A clear shift in the corresponding histogram can be observed as a significant fraction of the carriers now exhibit lifetime above 400 µs. The maximum lifetime was observed around 580 µs (refer to histogram in Fig. 8(b)).

The precursor samples used in this work are presumably good quality industrial TOPCon samples with high lifetime, and iV_{oc} i.e., with excellent individual layer properties and surface passivation from both

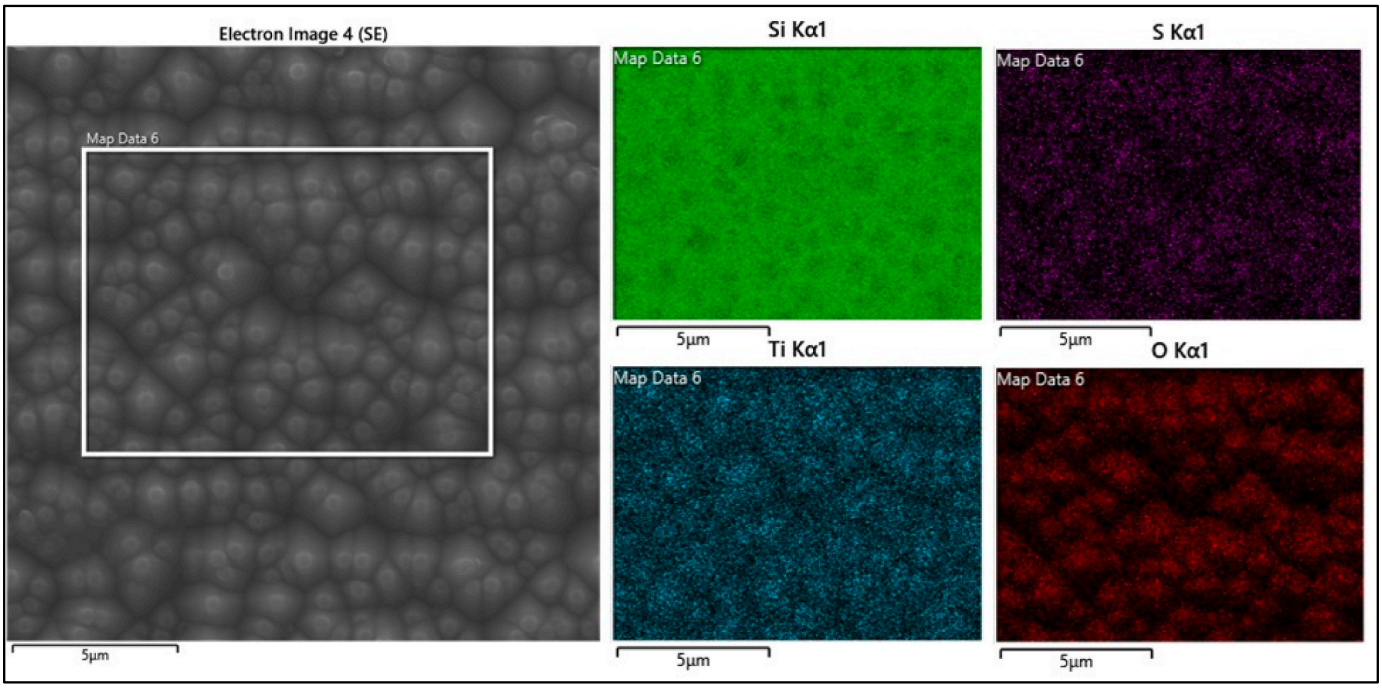

Fig. 5. SEM image (left), under magnification, highlighting the surface morphology of TiO_2 deposited area accompanied with corresponding EDS mapping of selected region (white box) to confirm elemental composition.

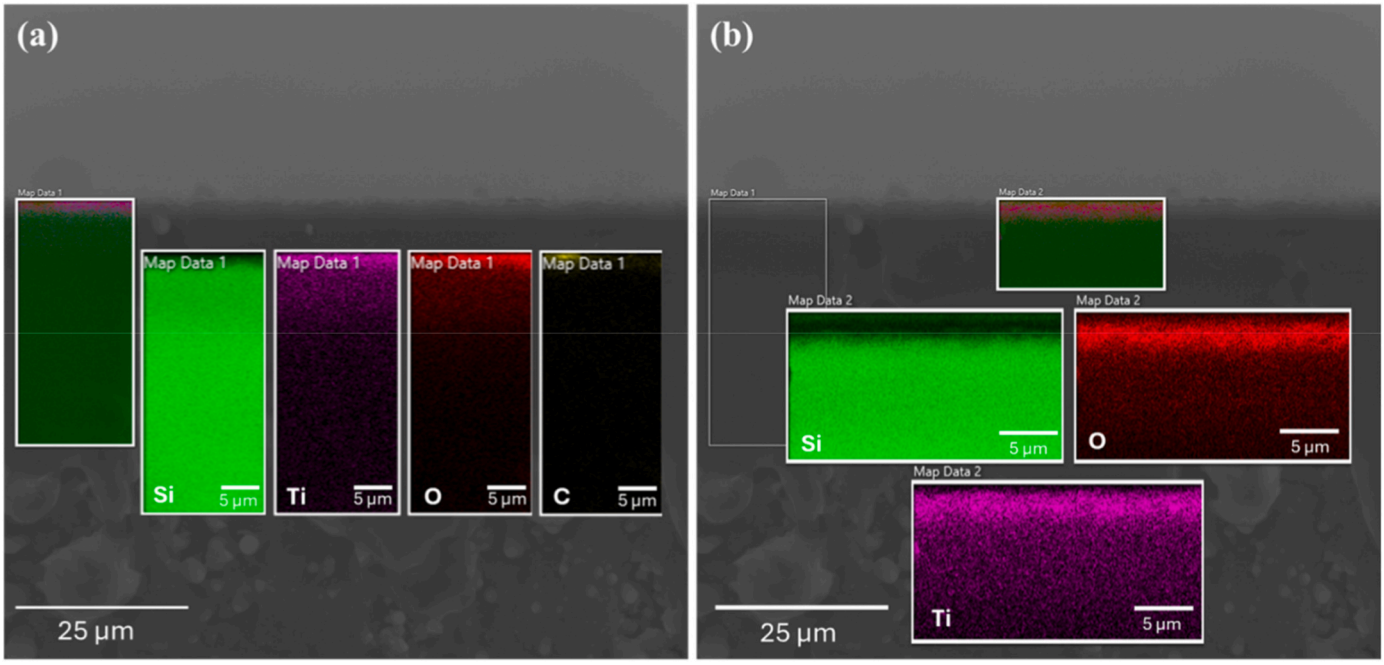

Fig. 6. EDS mapping of the TiO_2 layer in two different regions (a) and (b) of the cross section of the passivated sample. Presence of Ti (purple) and O (red) towards the surface is seen. (For interpretation of the references to color in this figure legend, the reader is referred to the Web version of this article.)

sides. Once these high-quality samples are cut using laser scribing, defects are introduced at the newly formed edges, majorly in the bulk part of the edges. These defects inherently drive the carriers towards them or in other words the carriers generated in the center diffuse towards these defects and recombine rapidly there. In addition, due to the small size of the sample this process is more pronounced, since the carriers have a shorter diffusion path to the edge. Therefore, despite the fact that these pieces come from high quality precursors and the bulk around the center is good, the measured lifetime is decreased by edge recombination. Once the edges are passivated, these defects no longer act as sinks for the carriers and the carriers from the center no longer diffuse towards these states, effectively increasing carrier lifetime at the center (Fig. 8 (b)).

Annealing at 180 °C further improved the passivation ability of the deposited film therefore lifetime at the center was further increased, as the color of the topogram changes to dark blue (Fig. 8(c)), highlighting the lifetime of >600 µs in these regions which can be seen in the histogram also as some fresh fraction now occupy lifetime ≥600 µs. Further annealing at 200 °C and 215 °C deteriorate the lifetime, as the maximum observed lifetime around the center falls below 600 µs and 575 µs, respectively. These lifetime topograms are in line with the observed

Table 1
Device parameters after passivation layer (TiO_2) deposition followed by annealing for 10 min at different temperatures.

Measurement	Lifetime at 1×10^{15} (μs)	Lifetime at V_{mpp} (μs)	iV_{oc} (mV)	iFF (%)
Before edge passivation	724	668	715.0	84.82%
After edge passivation	823	763	717.1	85.12%
After annealing at 180 °C	873	829	723.6	84.72%
After annealing at 200 °C	800	743	720.1	84.69%
After annealing at 215 °C	789	732	721.8	84.43%

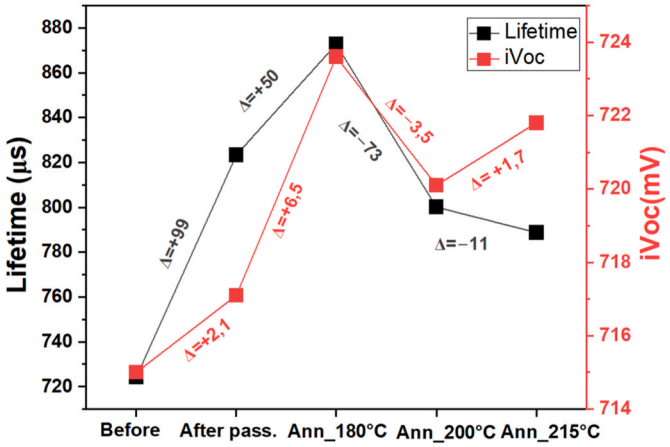

Fig. 7. Variation in lifetime and iV_{oc} of the passivated sample under different experimental conditions. Δ for each data point refers to the change in lifetime (black) and iV_{oc} (red) with the same units as stated on the axes. (For interpretation of the references to color in this figure legend, the reader is referred to the Web version of this article.)

lifetime from Sinton WCT-120PL, as a similar pattern was observed in the sample lifetime post annealing at 200 °C and 215 °C. All the gains observed in lifetime after deposition and annealing at 180 °C are lost after annealing at 215 °C. This effect may be attributed to the induced crystallinity in the TiO_2 layer through annealing at higher temperatures, as detailed later in the discussion section.

3.4. Annealing experiment

To understand the impact of annealing on the sample passivation, five non-passivated samples were annealed for 10 min at different temperatures from 150 °C to 215 °C. The first two samples (Ann_all_1 and Ann_all_2) were annealed together at 150 °C, 180 °C, 200 °C and 215 °C to mimic the experiments done with the edge passivated sample. While the other three samples, Ann_180 °C, Ann_200 °C and Ann_215 °C, were annealed at only one temperature each namely 180 °C, 200 °C and 215 °C, respectively. The results are tabulated in Table 2 and lifetime gains observed for these samples are displayed in Fig. 9. It is observed that annealing does have some impact on these scribed samples, as increasing lifetimes are observed for each sample, mainly due to possibility of some SiO_2 formation at dangling bonds created after laser scribing. This gain may also be attributed to the re-arrangement of defect states under exposure to moderate annealing temperature. Post annealing, lifetime exhibited nearly uniform increment at these annealing temperatures. Samples, Ann_all_1 and Ann_all_2, which were annealed subsequently at all these temperatures exhibited almost similar gains of 61 μs and 60 μs. It is worth to mention that only annealing at 180 °C (Ann_180 °C, Δ = 36 μs) resulted in nearly identical gain to that of annealing at 150 °C followed by 180 °C (Ann_all_1, Δ = 32 μs and Ann_all_2, Δ = 39 μs). It means annealing at 180 °C is sufficient to passivate native bonds through thermal energy. This is further supported by the gain (Δ = 36 μs) observed for Ann_200 °C. For a passivated-annealed sample, the lifetime was increased by 149 μs after deposition of passivation layer at 150 °C followed by annealing at 180 °C whereas the increment for only annealed sample Ann_180 °C was 36 μs. This illustrates the impact of local passivation on the scribed samples. It is worth mentioning that the precursor cells used here are TOPCon samples which are usually processed at higher temperatures (processes like emitter formation, deposition of poly-Si and activation of SiN_x, Al_2O_3) [4,35,36] than the present experimental temperature ranges. Therefore, the relatively low temperature range used here is not expected to alter the passivation characteristics at other interfaces. Therefore, improvements in the lifetime observed here can be directly correlated to the carrier behavior at the scribed edges.

In addition to this, one additional non-passivated sample Ann_150 °C (Table 2), was annealed at 150 °C for a duration of 1 h 40 min, equivalent to the deposition time of TiO_2 layer on the passivated sample, in order to separate out the role of temperature exposure to the passivated sample during passivation. After annealing, a lifetime gain of 46 μs is observed which is lower than the overall gains observed for passivated samples. Nonetheless, prolonged exposure duration (in comparison to Ann_all_1 and Ann_all_2) very marginally increased the carrier lifetime. These observations with different annealing experiments further elucidates the impact of localized passivation on the scribed sample.

4. Discussion

The present work aims to innovate the edge passivation process, usually carried out for minimizing the recombination activity at the newly cut edges formed during the halving and shingling of the industrial solar cells for applications in half cut and shingle modules. Unlike the complete blanket type layer formation in edge cut cells (Fig. 1(b) and (c)), the present work utilizes Direct Atomic Layer Processing (DALP®) technology to locally passivate the edges. DALP® leverages ALD with a miniaturized nozzle system enabling direct deposition of highly conformal passivation layers in the targeted areas. Therefore, using DALP®, a 230–240 μm wide and 50 nm thick TiO_2 layer was deposited successfully along the edges (Fig. 2) on the front side (emitter side) of the laser scribed TOPCon cell piece. Due to some limitations of the current sample holder stage, the layer deposition was limited to ~10 μm in the cross section, which will be targeted to cover the entire cross section in the future works. Even with the limited exposure in the cross section, the lifetime data of the passivated samples (Table 1) clearly indicates improvements in the sample lifetime post TiO_2 deposition and after annealing at 180 °C. Deposition of 50 nm TiO_2 film at 150 °C leads to an increment of 99 μs which is further improved by 50 μs after annealing at 180 °C. However, further annealing at 200 °C and 215 °C, deteriorates the passivation quality thereby decreasing the carrier lifetime.

This non-monotonic behavior of TiO_2 edge passivation can be mainly attributed to competing physical and chemical processes at the interface. As-deposited film, owing to the amorphous nature of it, efficiently suppresses the dangling bond density at the edges. Especially, TTIP grown films have shown good amount of atomic hydrogen (for example ~9.15 at.% in Ref. [37]). D. Hiller et al., [37] examined the passivation ability of TiO_2 using different precursors viz. TTIP, $TiCl_4$ and TDMAT and attributed the TTIP-TiO_2 passivation to the H content in the films. Further, the alkoxide groups in TTIP may also help to form SiO_x on the H terminated Si bonds at the edges. However, as deposited TiO_2 may contain some structural disorders within the film which undergoes

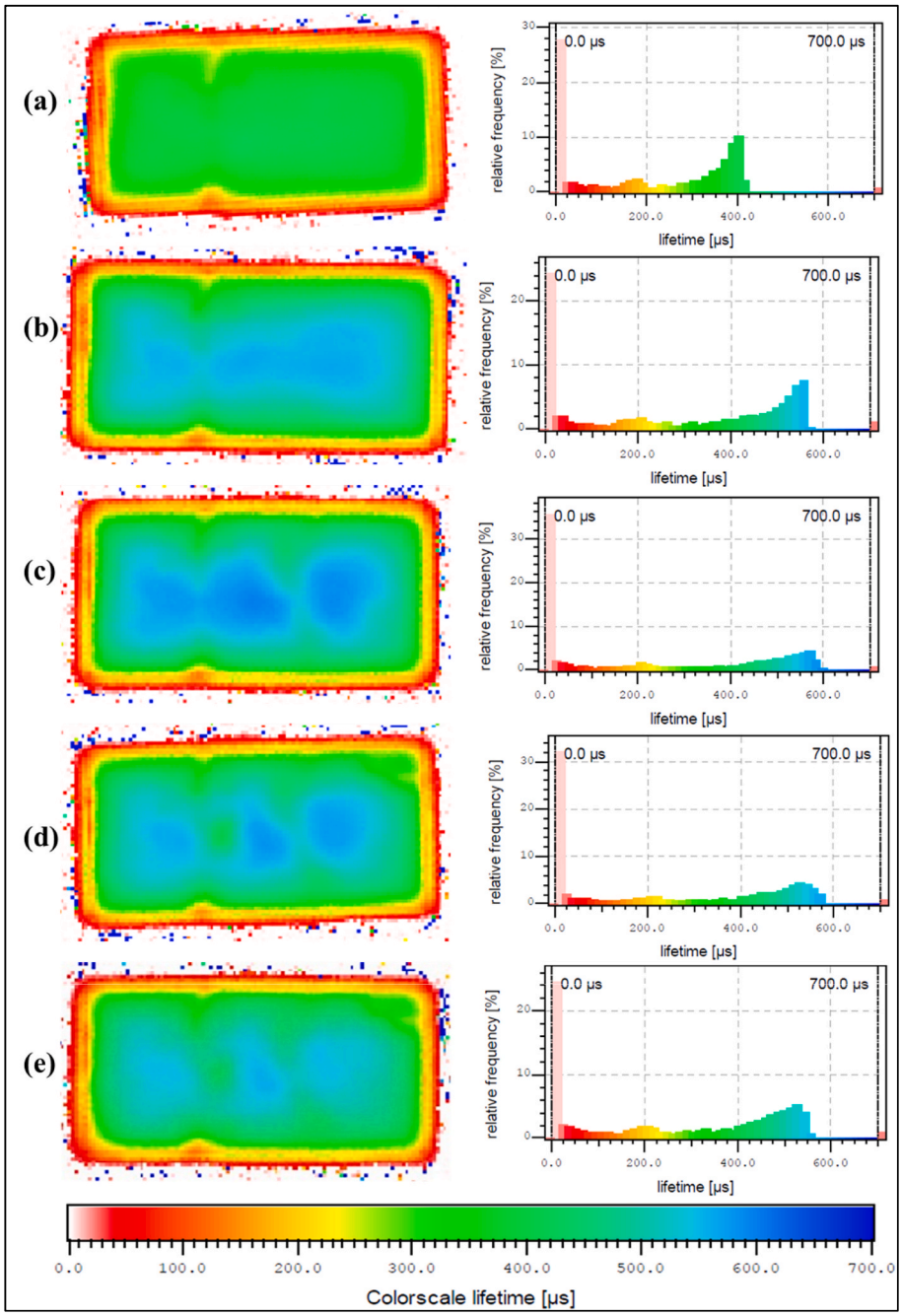

Fig. 8. Lifetime mapping results with corresponding histogram for passivated sample (a) before passivation, (b) after passivation, (c) after annealing at 180 °C, (d) after annealing at 200 °C and (e) after annealing at 215 °C.

partial rearrangement under mild annealing and re-arranges the TiO_2 network, further reducing the defect density at the interface. The thermal annealing also activates the movement of H atom which also helps in further suppression of dangling bond density. This is strongly supported by the gains observed in the lifetime post TiO_2 deposition and annealing at 180 °C. However, further annealing at higher temperatures of the 200 °C and 215 °C degraded the passivation ability of the film hence decreasing the carrier lifetime (Table 1 and Fig. 8(d) and (e)). This pattern may have resulted from the phase transformation of deposited film from amorphous to crystalline phase. In fact, most of the works examining surface passivation ability of ALD deposited TiO_2 on silicon surfaces identified low temperature grown film as more beneficial. Low temperature supports amorphous growth of the film which passivates the surface more effectively as compared to the crystalline films [38–40]. The transition temperature from amorphous to the crystalline is quite low (from 180 °C to 250 °C) for TiO_2 films and may vary depending on the deposition conditions [38,39,41]. This transition temperature also has dependency on the type of precursors used [37,42]. TTIP grown films, in particular, are found to be more crystalline when compared to $TiCl_4$. Other than precursors, thickness of the film also greatly influences the onset for the phase transformation [32,40,43], and the crystallization generally occurs at lower temperature for the thicker films [40].

Therefore, higher annealing temperature, on one hand, can rupture H-passivated bonds causing re-appearance of dangling bonds and on the other, induces crystallinity in the TiO_2 films. Suh et al., [34] also observed similar patterns with stacked Al_2O_3/TiO_2 film, where annealing of TiO_2 film led to degradation of passivation quality which they

Table 2
Lifetime data of non-passivated samples annealed at different temperatures for a duration of 10 min at each set temperature.

Sample	Lifetime (μs) at carrier injection of 1×10^{15} cm^{-3}					
	Before Annealing	After annealing at				Gains[b]
		150 °C	180 °C	200 °C	215 °C	
Ann_all_1	387	406	419	427	448	
Δ		+19	+13	+8	+21	= 61
Ann_all_2	393	409	432	447	453	
Δ		+16	+23	+15	+6	= 60
Ann_180 °C	354		390			
Δ			+36			= 36
Ann_200 °C	363			399		
Δ				+36		= 36
Ann_215 °C	373				398	
Δ					+25	= 25
Ann_150 °C[a]	443	489				
Δ		+46				= 46

[a] Ann_150 °C was annealed at 150 °C for 1 h 40 min.
[b] Gains represent the sum of all increments after annealing at each temperature.

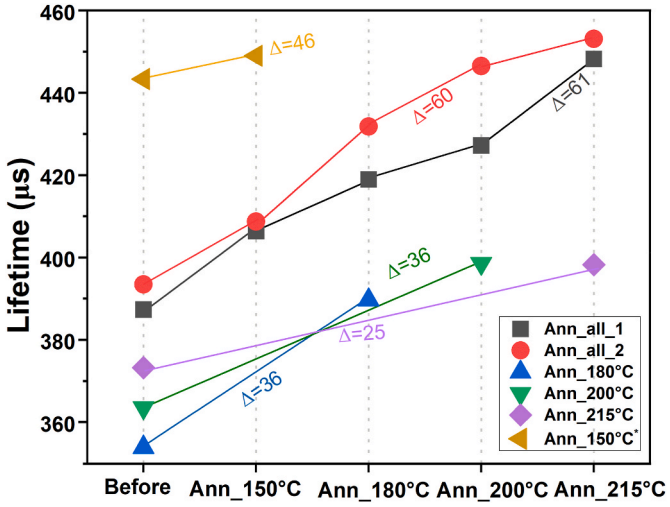

Fig. 9. Lifetime gains for only annealed (non-passivated) samples. Ann_all_1 and Ann_all_2 were annealed together from 150 °C to 215 °C for 10 min at each temperature. Ann_180 °C, Ann_200 °C and Ann_215 °C were annealed for 10 min at 180 °C, 200 °C and 215 °C, respectively. Ann_150 °C was annealed at 150 °C for 1 h 40 min, equivalent to the deposition time of passivated samples.

attributed to change in crystallinity or increased defect density within TiO_2 layer. With annealing, the crystallization of initial amorphous layers can lead to newly formed grain boundaries within the amorphous matrix which in turn may increase the density of carrier trapping defect sites [34]. In addition, the lower surface passivation for the crystalline phases can also be due to rupturing of Si-O-Ti bonds [39,44] or to the relatively high tensile stress in the crystallization process [45].

Therefore, it is quite plausible that induced crystallinity in the deposited film resulted in degradation of passivation quality after annealing at elevated temperatures. Further, owing to the higher thickness, TiO_2 film in present case is more prone to the induced crystallization and subsequently more sensitive to the annealing temperatures [46,47]. This was also observed in the lifetime topogram, where clear change in lifetime was observed after annealing.

It is important to point out that, even with localized nature of deposited film, covering a very small fraction of the total front surface of device, a significant improvement of 149 μs in lifetime and a gain of 8.6 mV in implied open circuit voltage (iV_{oc}) are obtained, effectively highlighting that local edge passivation through TiO_2 can be a better way to passivate the dangling bonds induced by laser scribing. DALP® is not limited to only TiO_2 depositions but can be used to deposit different metal-oxides. Hence, our future work will explore the local edge passivation with Al_2O_3 film.

5. Conclusion

Cutting cells into smaller bits, for e.g. shingling interconnection effectively minimizes some of the major power losses observed at the module level for high efficiency cells, however, the increased charge carrier recombination at the native edges created by the cell cutting process is a challenge. To overcome these losses, edge passivation must be optimized. In this work, we used Direct Atomic Layer Processing (DALP®) technology with the NANOFABRICATOR® tool from ATLANT 3D to innovate the edge passivation process through locally depositing TiO_2 films in the laser scribed areas. Using this tool, a very thin blanket layer of TiO_2 with ~230–240 μm width is deposited locally around the edges. This layer also extends to ~10 μm in the cross section which is expected to effectively wrap the top junction region as well. EDS mapping has confirmed the presence of TiO_2 in the intended regions. TiO_2 layer was deposited at 150 °C using TTIP as precursor and water as the co-reactant. Post passivation, improvements in lifetime and iV_{oc} are observed for the scribed device. The lifetime was increased by 99 μs and iV_{oc} by 2.1 mV. Further annealing at 180 °C improved the device parameters as a gain of 50 μs and 6.5 mV in lifetime and iV_{oc} was observed. However, subsequent annealing at 200 °C and 215 °C decreased the device lifetime and iV_{oc}. This pattern can be attributed to the induced crystallinity in the deposited film with thermal annealing at higher temperatures. Amorphous TiO_2 is known to suppress the dangling bond density more effectively than the crystalline phase.

In comparison to the passivated samples, only annealed samples (non-passivated) exhibited a lower gain under different annealing conditions. Even for the samples annealed in the entire temperature range i.e. from 150°C to 215 °C the carrier lifetime was only increased by ~60 μs. This entails the effectiveness of locally deposited TiO_2 layer around the edges. The observed results suggest that local edge passivation can turn out to be a good choice for reducing recombination activity around the edges.

CRediT authorship contribution statement

Dheeraj Sah: Writing – review & editing, Writing – original draft, Methodology, Investigation, Formal analysis, Conceptualization. **Karolis Parfeniukas:** Writing – review & editing, Writing – original draft, Methodology, Investigation, Conceptualization. **Roberto Boccardi:** Writing – review & editing, Methodology, Investigation. **Narendra Bandaru:** Writing – review & editing, Investigation. **Agata Lachowicz:** Writing – review & editing. **Bertrand Paviet- Salomon:** Writing – review & editing, Validation. **Benjamin Borie:** Writing – review & editing, Resources. **Mira Baraket:** Writing – review & editing, Resources. **Maksym Plakhotnyuk:** Writing – review & editing, Resources, Funding acquisition. **Gisele A. Dos Reis Benatto:** Writing – review & editing, Validation. **Sune Thorsteinsson:** Writing – review & editing, Validation, Project administration. **Peter B. Poulsen:** Project administration, Funding acquisition. **Rasmus Schmidt Davidsen:** Writing – review & editing, Validation, Supervision, Project administration, Funding acquisition, Conceptualization.

Declaration of competing interest

The authors declare that they have no known competing financial interests or personal relationships that could have appeared to influence the work reported in this paper.

Acknowledgement

The present work is supported by Innovation Fund Denmark under

the "ACES- Advanced Contact Engineering and Surface Passivation" for Solar Cells with grant number 3148-00044B.

Data availability

Data will be made available on request.

References

[1] G. Masson, A. Jager-Waldau, I. Kaizuka, J. Lindahl, J. Donoso, M. de L'Epine, A snapshot of the global PV market and industry. In 2025 IEEE 53rd Photovoltaic Specialists Conference (PVSC) (pp. 508-510).

[2] SolarPower Europe, Global Market Outlook for Solar Power 2025-2029, 2025.

[3] M.A. Green, E.D. Dunlop, M. Yoshita, N. Kopidakis, K. Bothe, G. Siefer, X. Hao, J. Y. Jiang, Solar cell efficiency tables (version 66), Prog. Photovoltaics Res. Appl. 33 (2025) 795–810.

[4] C. Ballif, F.J. Haug, M. Boccard, P.J. Verlinden, G. Hahn, Status and perspectives of crystalline silicon photovoltaics in research and industry, Nat. Rev. Mater. 7 (8) (2022) 597–616.

[5] H. Hanifi, C. Pfau, D. Dassler, J. Schneider, S. Schindler, M. Turek, J. Bagdahn, Investigation of cell-to-module (CTM) ratios of PV modules by analysis of loss and gain mechanisms, Photo Interpret. 32 (2016) 89–99.

[6] G. Beaucarne, Materials challenge for shingled cells interconnection, Energy Proc. 98 (2016) 115–124.

[7] M. Mittag, A. Pfreundt, J. Shahid, N. Wöhrle, D.H. Neuhaus, Techno-economic analysis of half-cell modules: the impact of half cells on module power and costs, in: 36th European Photovoltaic Solar Energy Conference and Exhibition, EU PVSEC), 2019, September, pp. 1032–1039.

[8] M. Mittag, T. Zech, M. Wiese, D. Blasi, M. Ebert, H. Wirth, Cell-to-Module (CTM) analysis for photovoltaic modules with shingled solar cells, in: 2017 IEEE 44th Photovoltaic Specialist Conference (PVSC), IEEE, 2017, June, pp. 1531–1536.

[9] D. Tonini, G. Cellere, M. Bertazzo, A. Fecchio, L. Cerasti, M. Galiazzo, Shingling technology for cell interconnection: technological aspects and process integration, Energy Proc. 150 (2018) 36–43.

[10] P. Baliozian, N. Klasen, N. Wöhrle, C. Kutter, H. Stolzenburg, A. Münzer, P. Saint-Cast, M. Mittag, E. Lohmüller, T. Fellmeth, M. Al-Akash, A. Kraft, M. Heinrich, A. Richter, A. Fell, A. Spribille, H. Neuhaus, R. Preu, PERC-based shingled solar cells and modules at fraunhofer ISE, Photo Interpret. 43 (2019) 129–145.

[11] P. Baliozian, E. Lohmüller, T. Fellmeth, N. Wöhrle, A. Krieg, R. Preu, Bifacial shingle solar cells on p-type Cz-Si (pSPEER), in: AIP Conference Proceedings, 1999, AIP Publishing, 2018, August, 1.

[12] S. Harrison, B. Portaluppi, P. Bertrand, V. Giglia, B. Martel, A. Sekkat, D. Munoz-Rojas, Low temperature post-process repassivation for heterojunction cut cells, in: 38th European Photovoltaic Solar Energy Conference and Exhibition, 2021, pp. 167–171.

[13] M. Albaric, B. Martel, S. Harrison, S. Edouard, Process optimization for edge passivation and high efficiency shingle heterojunction cells compatible with industry, in: EU PVSEC 2023-40th European Photovoltaic Solar Energy Conference & Exhibition, 2023, September.

[14] B. Martel, M. Albaric, S. Harrison, F. Dhainaut, T. Desrues, Addressing separation and edge passivation challenges for high efficiency shingle heterojunction solar cells, Sol. Energy Mater. Sol. Cell. 250 (2023) 112095.

[15] S. Harrison, A. Bettinelli, B. Portaluppi, V. Giglia, C. Carrière, A. Sekkat, D. Munoz-Rojas, V. Barth, Challenges for Efficient Integration of SHJ Based Solar Cells in Shingle Module Configuration, 37th EU PVSEC, 2020, pp. 223–227.

[16] J. Lelièvre, S. Harrison, M. Albaric, L. Carton, B. Portaluppi, V. Barth, Alternative CZ ingot squaring and half-cell cutting methodology for low-temperature PV cell and module technologies, in: Proc. 37th Eur. Photovolt. Sol. Energy Conf, 2020, pp. 487–489.

[17] S.W. Glunz, J. Dicker, M. Esterle, M. Hermle, J. Isenberg, F.J. Kamerewerd, J. Knobloch, D. Kray, A. Leimenstoll, F. Lutz, D. OBwald R. Preu, S. Rein, E. Schaffer, C. Schetter, H. Schmidhuber, H. Schmidt, M. Steuder, C. Vorgrimler, G. Willeke, High-efficiency silicon solar cells for low-illumination applications, in: Proc. 29th IEEE PVSC, 2002, pp. 450–453. New Orleans, Louisiana, USA.

[18] W.P. Mulligan, A. Terao, D.D. Smith, P.J. Verlinden, R.M. Swanson, Development of chip-size silicon solar cells, in: Proc. 28th IEEE PVSC, 2000, pp. 158–163. Anchorage, Alaska, USA.

[19] A. Münzer, P. Baliozian, A. Steinmetz, T. Geipel, S. Pingel, A. Richter S. Roder, E. Lohmuller, A. Spribille, R. Preu, Post-separation processing for silicon heterojunction half solar cells with passivated edges, IEEE J. Photovoltaics 11 (6) (2021) 1343–1349.

[20] S. Harrison, V. Barth, C. Carrière, M. Albaric, B. Martel, M. Galiazzo, E. Sovernigo, N. Frasson, Simplified cell cutting, efficient edge passivation, copper metallization: tackling the last hurdles for optimized SHJ integration in shingle module configuration. Proceedings of the 8th WCPEC, 2022.

[21] E. Lohmüller, P. Baliozian, L. Gutmann, L. Kniffk, A. Richter, L. Wang, R. Dunbar, A. Lepert, J.D. Huyeng, R. Preu, TOPCon shingle solar cells: thermal laser separation and passivated edge technology, Prog. Photovoltaics Res. Appl. 31 (7) (2023) 729–737.

[22] E. Lohmüller, P. Baliozian, L. Gutmann, L. Kniffki, V. Beladiya, J. Geng, L. Wang, R. Dunbar, A. Lepert, M. Hoffman, A. Richter, J.D. Huyeng, Thermal laser separation and high-throughput layer deposition for edge passivation for TOPCon shingle solar cells, Sol. Energy Mater. Sol. Cell. 258 (2023) 112419.

[23] W. Li, R. Zhou, Y. Wang, Q. Su, J. Yang, M. Xi, Y. Liu, Preparation of Al2O3 thin films by RS-ALD and edge passivation application for TOPCon half solar cells, Appl. Surf. Sci. 673 (2024) 160835.

[24] R. Zhou, W. Li, B. Ge, J. Song, Q. Su, M. Xi, Y. Liu, Optimization of the deposited Al2O3 thin film process by RS-ALD and edge passivation applications for half-solar cells, Ceram. Int. (2024).

[25] B. Portaluppi, S. Harrison, V. Giglia, A. Sekkat, D. Munoz-Rojas, Insights on cell edge defects impact and post-process repassivation for heterojunction, in: Proceedings of the 37th European Photovoltaic Solar Energy Conference and Exhibition, 2020, pp. 504–507.

[26] C. Leon, D. Barakel, V. Burlac, L. Roux, R.B. Abbes, T. Regrettier, O. Palais, F. Torregrosa, Ion implantation investigation for the passivation of cut edge solar cells, in: AIP Conference Proceedings, 2826, AIP Publishing, 2023, June. No. 1.

[27] X. Wang, X. Zhang, Y. Bai, W. Li, B. Chen, J. Guo, X. Yang, X. Yan, S. Wang, J. Chen, Development of passivating edge shingle modules with right cut, new loss evaluation and liquid-based edge passivation strategy, Sol. Energy Mater. Sol. Cell. 261 (2023) 112513.

[28] W. Li, X. Wang, J. Guo, X. Zhang, B. Chen, J. Chen, Q. Gao, X. Yang, F. Li, J. Wang, D. Song, S. Wang, H. Li, J. Chen, Compensating cutting losses by passivation solution for industry upgradation of topcon and shj solar cells, Adv. Energy Sustain. Res. 4 (2) (2023) 2200154.

[29] I. Kundrata, M.K. Barr, S. Tymek, D. Döhler, B. Hudec, P. Brüner, G. Vanko, M. Precner, T. Yokosawa, E. Spiecker, M. Plakhotnyuk, J. Bachmann, Additive manufacturing in atomic layer processing mode, Small Methods 6 (5) (2022) 2101546.

[30] S. Santucci, A. Kinikar, Z. Wang, N.S. Ruhela, J. Navne, M. Akbari, A. Mishchenko, M. Baraket, M. Plakhotnyuk, Growth dynamics in patterned TiO2 deposited by direct atomic layer processing (DALP) in ambient conditions, J. Vac. Sci. Technol. A 43 (2025) 062411.

[31] J. Aarik, A. Aidla, T. Uustare, M. Ritala, M. Leskelä, Titanium isopropoxide as a precursor for atomic layer deposition: characterization of titanium dioxide growth process, Appl. Surf. Sci. 161 (3–4) (2000) 385–395.

[32] Q. Xie, J. Musschoot, D. Deduytsche, R.L. Van Meirhaeghe, C. Detavernier, S. Van den Berghe, Y.-L. Jiang, G.-P. Ru, B.-Z. Li, X.P. Qu, Growth kinetics and crystallization behavior of TiO2 films prepared by plasma enhanced atomic layer deposition, J. Electrochem. Soc. 155 (9) (2008) H688.

[33] M.M. Plakhotnyuk, N. Schüler, E. Shkodin, R.A. Vijayan, S. Masilamani, M. Varadharajaperumal, A. Crovetto, O. Hansen, Surface passivation and carrier selectivity of the thermal-atomic-layer-deposited TiO2 on crystalline silicon, Jpn. J. Appl. Phys. 56 (8S2) (2017).

[34] D. Suh, D.Y. Choi, K.J. Weber, Al2O3/TiO2 stack layers for effective surface passivation of crystalline silicon, J. Appl. Phys. 114 (15) (2013).

[35] B.V. Stefani, M. Kim, Y. Zhang, B. Hallam, M.A. Green, R.S. Bonilla, C. Fell, G. J. Wilson, M. Wright, Historical market projections and the future of silicon solar cells, Joule 7 (12) (2023) 2684–2699.

[36] S.W. Glunz, B. Steinhauser, J.I. Polzin, C. Luderer, B. Grübel, T. Niewelt, A.M.O. M. Okasha, M. Bories, H. Nagel, K. Krieg, F. Feldmann, A. Richter, M. Bivour, M. Hermle, Silicon-based passivating contacts: the TOPCon route, Prog. Photovoltaics Res. Appl. 31 (4) (2023) 341–359.

[37] D. Hiller, F. Munnik, J. López-Vidrier, D. Solonenko, J. Reif, M. Knaut, O. Thimm, N.E. Grant, Comparison of three titanium-precursors for atomic-layer-deposited TiO2 for passivating contacts on silicon, J. Vac. Sci. Technol. A 42 (2024) 032406.

[38] I.S. Yu, I.-H. Chang, H.E. Cheng, Y.S. Lin, Surface passivation of c-Si by atomic layer deposition TiO 2 thin films deposited at low temperature, in: 2014 IEEE 40th Photovoltaic Specialist Conference (PVSC), IEEE, 2014, pp. 1271–1274.

[39] L. Zhaoheng, J. He, X. He, M. Liao, P. Liu, Z. Yang, J. Ye, P. Gao, Excellent passivation of silicon surfaces by thin films of electron-beam-processed titanium dioxide, IEEE J. Photovoltaics 7 (6) (2017) 1551–1555.

[40] L. Wensheng, J. Tong, P. Narangari, S. Armand, T.C. Kho, M. Ernst, D. Walter, S. R. Surve, K.R. McIntosh, M. Stocks, K.J. Weber, A. Blakers, K.C. Fong, Impact of Al Doping on Surface Passivation of TiO x on Si, IEEE J. Photovoltaics 10 (4) (2020) 940–944.

[41] M. Plakhotnyuk, A. Crovetto, O. Hansen, Behind the nature of titanium oxide excellent surface passivation and carrier selectivity of c-Si, in: 26th International Photovoltaic Science and Engineering Conference, 2016.

[42] I. Jõgi, M. Pärs, J. Aarik, A. Aidla, M. Laan, J. Sundqvist, L. Oberbeck, J. Heitmann, K. Kukli, Conformity and structure of titanium oxide films grown by atomic layer deposition on silicon substrates, Thin Solid Films 516 (15) (2008) 4855–4862.

[43] W.D. Kim, G.W. Hwang, O.S. Kwon, S.K. Kim, M. Cho, D.S. Jeong, S.W. Lee, M. H. Seo, C.S. Hwang, Y.-S. Min, Y.J. Cho, Growth characteristics of atomic layer deposited TiO2 thin films on Ru and Si electrodes for memory capacitor applications, J. Electrochem. Soc. 152 (8) (2005) C552.

[44] G. Sahasrabudhe, S.M. Rupich, J. Jhaveri, A.H. Berg, K.A. Nagamatsu, G. Man, Y. J. Chabal, A. Kahn, S. Wagner, J.C. Sturm, J. Schwartz, Low-temperature synthesis of a TiO2/Si heterojunction, J. Am. Chem. Soc. 137 (47) (2015) 14842–14845.

[45] B. Liao, B. Hoex, A.G. Aberle, D. Chi, C.S. Bhatia, Excellent c-Si surface passivation by low-temperature atomic layer deposited titanium oxide, Appl. Phys. Lett. 104 (2014) 253903.

[46] Y. Nakagawa, K. Gotoh, T. Inoue, Y. Kurokawa, N. Usami, Improved performance of titanium oxide/silicon oxide electron-selective contacts by implementation of magnesium interlayers, Phys. Status Solidi. 218 (19) (2021) 2100296.

[47] J. Aarik, A. Aidla, H. Mändar, T. Uustare, M. Schuisky, A. Hårsta, Atomic layer growth of epitaxial TiO_2 thin films from $TiCl_4$ and H_2O on α-Al2O3 substrates, J. Cryst. Growth. 242 (1–2) (2002) 189–198.